Phase diagram of a system of hard spherocylinders by computer simulation

J. A. C. Veerman and D. Frenkel
FOM–Institute for Atomic and Molecular Physics, P.O. Box 41883, 1009 DB Amsterdam, The Netherlands
(Received 12 October 1989)

We report a computer-simulation study of the phase diagram of a system of hard spherocylinders with aspect ratio L/D between 0 and 5. For $L/D \leq 3$ only isotropic liquid and crystalline solid phases can occur. For $L/D=3$ a mechanically stable smectic phase occurs, but it is thermodynamically unstable. For larger L/D values, stable smectic and nematic phases are present.

I. INTRODUCTION

Computer simulations have proved very useful in obtaining an understanding of the physical phenomena in atomic and molecular systems. The first computer simulations focused mainly on atomic systems, i.e., systems in which the particles interact through spherically symmetric potentials. Subsequently, simulations on systems with particles interacting through nonspherically symmetric particles ("molecular systems") have been performed. Such simulations allow us to gather insight into the ordering phenomena that are typical for molecular systems, e.g., liquid crystals. Most liquid-crystal forming molecules are quite complex. Surprisingly enough, however, many liquid-crystalline phases can be modeled using simple hard-core molecules. Therefore computer simulations on hard-core systems have been a subject of interest for some time.[1] Phase diagrams for various systems, such as hard ellipsoids[2] and hard parallel spherocylinders,[3] have been calculated. In the ellipsoid system three different phases occur: isotropic, nematic, and solid. An important question in literature[4] has been whether or not a stable smectic phase can occur in a system with a purely hard-core interaction. Numerical simulation of the phase diagram of the parallel spherocylinder system first showed unambiguous evidence that smectic order can occur in a hard-core system; apart from the nematic and solid phases, this system also displays a smectic and a columnar phase.

Recently[5] it was shown that also in a system of hard spherocylinders with a rotational degree of freedom ("free" hard spherocylinders) a stable smectic phase exists for the aspect ratio $L/D=5$. (Here D is the diameter of the cylinder and L is the length of the cylinder input in between the two hemispheres. The "total length" of the spherocylinder is $L+D$.) Recent density-functional calculations[6,7] predict that this stable smectic phase will exist for smaller L/D, together with a stable nematic phase. The isotropic-nematic-smectic triple point is predicted to occur at $L/D=3$ (Ref. 7) or $L/D=2.46$.[6]

In this study we report the results of computer simulations of hard-spherocylinder systems with $L/D=1$ and 3. Combining our data with the known results for $L/D=0$ (hard spheres[8]) and $L/D=5$ (Ref. 5) we obtain a tentative phase diagram of the spherocylinder system for $L/D \leq 5$.

II. CALCULATION OF THE PHASE DIAGRAM

In this section we summarize the procedure used to find the stable phases of a system of spherocylinders with a given L/D ratio.

A. Calculation of the equation of state

Knowledge of the equation of state often provides a rough estimate of the limits of stability of the various phases; by generating various different (i.e., ordered or disordered) starting configurations at different densities, the range of mechanical stability of the observed phases can be estimated. If only one phase is mechanically stable at a given density, this will also be the thermodynamically stable phase. If more phases appear to be mechanically stable, a free-energy calculation is needed to determine which phase is thermodynamically stable.

1. Numerical techniques

We prepared configurations of the dense spherocylinder system in three different ways.

(i) Compression of an isotropic liquid phase. At a low density a "stretched fcc lattice" (i.e., a fcc lattice in which all z coordinates are multiplied by a factor $(L/D+1)$ was "melted" by the application of constant-*NVT* (number, volume, temperature) Monte Carlo (*NVT*-MC) to the system. The ensuing isotropic liquid was thereupon compressed to a higher density by constant-*NPT* (number, pressure, temperature) Monte Carlo (*NPT*-MC) and allowed to equilibrate again by *NVT*-MC.

(ii) Expansion of a solid phase. At a density of 90% of closed packing a stretched fcc configuration was allowed to equilibrate by Monte Carlo. In this ordered phase at high density the box shape determines, to a considerable extent, what the "equilibrium" configuration will be. We therefore used a MC algorithm which allowed the box shape to fluctuate while keeping the box volume constant (variable-shape constant-volume Monte Carlo, or VSMC). Thus we allowed the system to determine its equilibrium box shape. The equilibrium configuration was subsequently expanded to a lower density and allowed to equilibrate again.

(iii) Starting from a parallel configuration. At some densities we started from a parallel spherocylinder

configuration (e.g., in a smectic state) and allowed it to equilibrate by VSMC. The ensuing equilibrium configuration was subsequently compressed by *NPT*-MC, or expanded, and allowed to equilibrate again.

After preparing a well-equilibrated configuration, the equation of state was determined by standard molecular dynamics[9] (MD). Typically, a MD run had about 400 collisions per particle (we used 240 particles in the $L/D=3$ system, and 144 particles in the $L/D=1$ system), which proved to be sufficient to determine the equation of state with reasonable accuracy. Near the density where we expected a phase transition to occur, we performed longer runs (1200–2000 collisions per particle), so that we were able to study the time evolution of nematic and smectic order parameter fluctuations.

2. Results

In Figs. 1 and 2 and Tables I and II we display the equations of state for $L/D=1$ and 3, respectively. (In the figures, $\rho^*=\rho/\rho_{cp}$ is the density relative to the density of close packing, also called the reduced density, and $P^*=Pv_0/kT$, where v_0 is the molecular volume.)

In the $L/D=1$ system we only find a liquid and a solid phase. The solid already melts at a density higher than that for which the smectic phase of the parallel $L/D=1$ system is stable.[3] This clearly suggests that no stable smectic phase occurs for this aspect ratio. We do not find a nematic phase either. This is consistent with the early observation of Vieillard-Baron[10] that a stable nematic phase does not exist for $L/D=2$.

In the $L/D=3$ system we find three mechanically stable phases: liquid, solid, and smectic. The smectic phase was obtained both by starting from a parallel configuration and by expanding the solid phase. When expanded, the solid transforms spontaneously into a smectic phase at a reduced density $\rho^*=0.64$. Upon compression the system remains in the smectic phase up to a density $\rho^*=0.70$, above which solidification occurs. Figure 3 shows the system in the smectic phase.

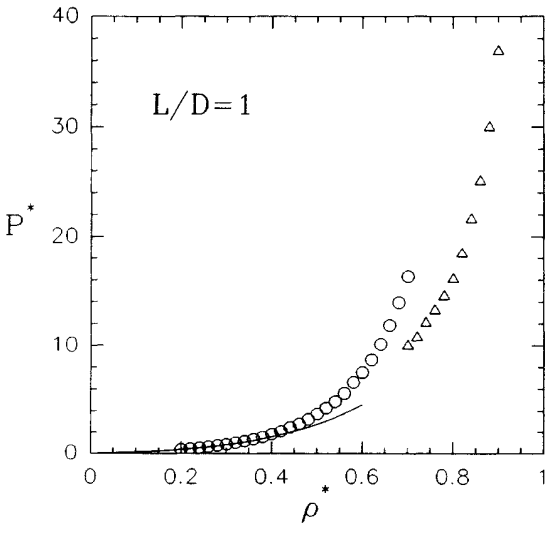

FIG. 1. Equation of state for $L/D=1$. The solid line represents the virial expansion to fourth order. B_3 and B_4 are taken from Ref. 1. The MD results for the isotropic fluid branch are represented by dots, the results for the solid branch are shown as triangles.

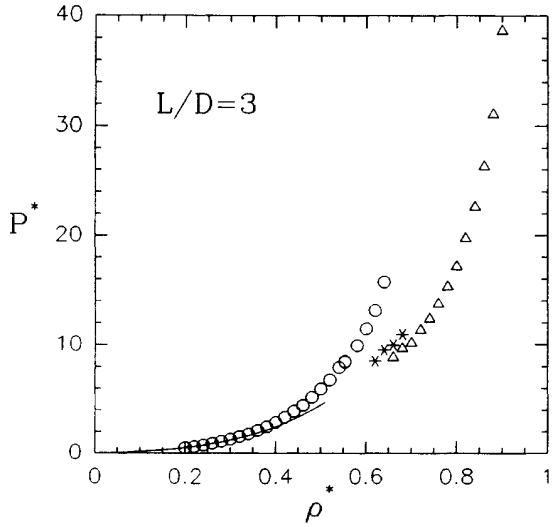

FIG. 2. Same as in Fig. 1 for $L/D=3$. The stars refer to the smectic branch.

When the liquid is compressed we see that the nematic order parameter S defined by

$$S=\tfrac{1}{2}\langle(3\cos^2\theta-1)\rangle \tag{1}$$

remains small (Table III), and we see no clear change in

TABLE I. Equation of state for the $L/D=1$ system.

Liquid		Solid	
ρ^*	Pv_0/kT	ρ^*	Pv_0/kT
0.20	0.374(6)	0.70	10.00(23)
0.22	0.450(5)	0.72	10.77(24)
0.24	0.533(8)	0.74	12.07(49)
0.26	0.630(6)	0.76	13.20(25)
0.28	0.736(5)	0.78	14.49(32)
0.30	0.859(15)	0.80	16.05(26)
0.32	1.009(13)	0.82	18.40(27)
0.34	1.174(20)	0.84	21.59(14)
0.36	1.366(24)	0.86	25.05(57)
0.38	1.556(41)	0.88	29.97(53)
0.40	1.834(27)	0.90	36.84(60)
0.42	2.090(38)		
0.44	2.457(66)		
0.46	2.790(69)		
0.48	3.239(52)		
0.50	3.740(54)		
0.52	4.288(82)		
0.54	4.88(14)		
0.56	5.62(12)		
0.58	6.63(14)		
0.60	7.54(25)		
0.62	8.72(25)		
0.64	10.15(28)		
0.66	11.88(34)		
0.68	13.94(48)		
0.70	16.32(56)		

TABLE II. Equation of state for the $L/D=3$ system.

Liquid		Smectic		Solid	
ρ^*	Pv_0/kT	ρ^*	Pv_0/kT	ρ^*	Pv_0/kT
0.20	0.517(8)	0.62	8.53(23)	0.66	8.82(21)
0.22	0.633(9)	0.64	9.54(16)	0.68	9.66(28)
0.24	0.762(13)	0.66	9.99(30)	0.70	10.17(15)
0.26	0.915(16)	0.68	10.97(36)	0.72	11.35(29)
0.28	1.093(22)	0.70	11.27(53)	0.74	12.37(26)
0.30	1.300(26)			0.76	13.74(46)
0.32	1.533(31)			0.78	15.28(27)
0.34	1.792(30)			0.80	17.14(29)
0.36	2.117(35)			0.82	19.75(40)
0.38	2.457(46)			0.84	22.62(45)
0.40	2.879(70)			0.86	26.31(44)
0.42	3.356(62)			0.88	31.07(32)
0.44	3.895(96)			0.90	38.66(53)
0.46	4.437(99)				
0.48	5.196(96)				
0.50	5.96(15)				
0.52	6.81(15)				
0.54	7.95(14)				
0.553	8.45(12)				
0.58	9.94(30)				
0.60	11.49(23)				
0.62	13.14(45)				
0.64	15.73(36)				

the slope of the equation of state. A dynamical study of the system reveals, however, that collective orientational fluctuations increase with increasing density in the isotropic phase; we studied the decay of the collective- and single-particle correlation functions and the static orientational correlation factor g_2. The single-particle orientational correlation function is defined by

$$C_2^s = \langle P_2(\mathbf{u}(0)\cdot\mathbf{u}(t))\rangle \ , \tag{2}$$

the collective orientation function by

$$C_2^c = \sum_{\substack{i,j \\ j\neq i}} \langle P_2(\mathbf{u}_i(0)\cdot\mathbf{u}_j(t))\rangle \ , \tag{3}$$

and the static orientational correlation factor by

$$g_2 = \sum_{\substack{i,j \\ j\neq i}} \langle P_2(\mathbf{u}_i\cdot\mathbf{u}_j)\rangle \ . \tag{4}$$

In order to study these quantities, MD runs were used with a length in the order of 40 time units, or 2000 collisions per particle. (Here time is measured in units of $D\sqrt{m/kT}$, where m is the mass of a particle and D the diameter of a cylinder.) Figure 4 shows that the ratio τ_2^c/τ_2^s of the decay times of the collective and single-particle correlation function and $1+g_2$ increase with increasing density, indicating that nematic fluctuations increase. Because the statistical errors in the decay times of the collective reorientational fluctuations are very large, we are unable to give an accurate estimate of the density of the isotropic-to-nematic transition, except that it is at some density $\rho^* > 0.60$. We also performed runs at reduced densities $\rho^* = 0.56$–0.60 starting from a parallel smectic configuration (smectic is the equilibrium phase for the parallel system at these densities). On these configurations we first applied 26 000–46 000 MC cycles to let the system "equilibrate," and subsequently MD for 40 time units to study the dynamics of the system. The

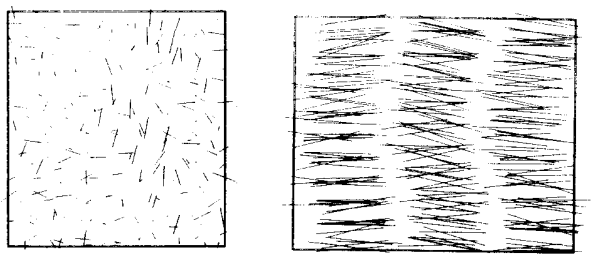

FIG. 3. Smectic configuration at a reduced density $\rho^* = 0.64$. The particles are represented by lines of length L. Left picture: top view. Right picture: side view.

TABLE III. Average nematic order parameter S defined by Eq. (1) as a function of the reduced density ρ^* for $L/D=3$ in the liquid branch.

ρ	S
0.52	0.065(15)
0.54	0.026(12)
0.553	0.045(42)
0.56	
0.58	0.131(23)
0.60	0.107(16)
0.62	0.060(11)
0.64	0.056(17)

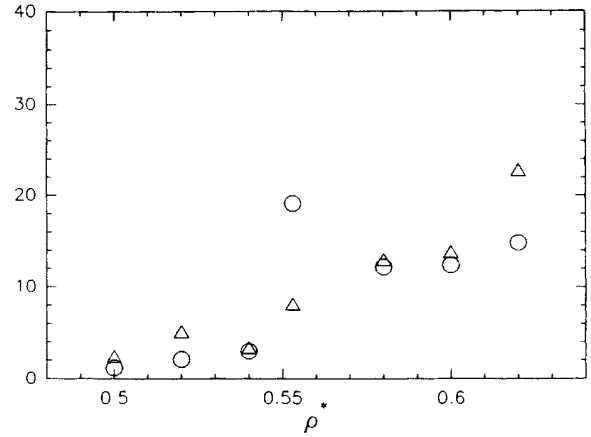

FIG. 4. t_2^c/t_2^s (dots) and $1+g_2$ (triangles) as a function of density for the compressed isotropic fluid. Here, t_2^c and t_2^s are the decay times of the collective and single-particle correlation functions, defined by Eqs. (2) and (3), and g_2 is the static correlation factor, defined by Eq. (4). Note that there is a gradual upward trend with increasing density.

values of the nematic order parameters at the start of the MD runs indicated that there was still nematic order present at the beginning of the MD run. Measurements of the decay of the collective orientational fluctuations indicate that even during the long MC run, equilibrium is not reached. During the MD simulation the system is still evolving towards the isotropic phase. Snapshots (Fig. 5) show configurations that look more like an isotropic fluid with remnants of a smectic phase than a true nematic phase. The decay to the isotropic phase becomes slower at higher density.

From these data it is not clear whether a small region exists in which a mechanically stable nematic phase occurs. Below we will show that the fact that the nematic phase can occur only for $\rho^* > 0.60$ implies that a thermodynamically stable nematic phase does not exist for $L/D=3$.

As we can see from Figs. 1 and 2, the isotropic, smectic, and solid phases are separated by first-order phase transitions with the concomitant hysteresis effects. In order to locate the thermodynamic coexistence points, free-energy calculations have to be performed.

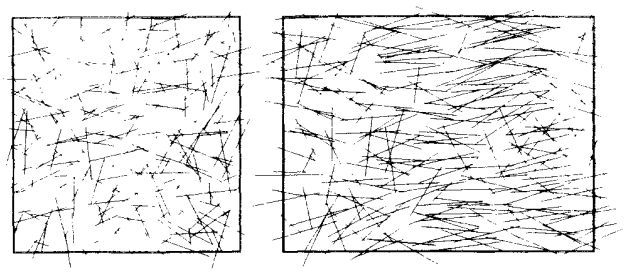

FIG. 5. Configuration of a spherocylinder system with $L/D=3$ at $\rho^*=0.58$, obtained by applying MC to a parallel configuration. The configuration showed is presumably a transient state from smectic to isotropic.

B. Free-energy calculations

1. Theory

The differences in the Helmholtz free energy of two thermodynamically stable points can be determined from the equation of state by the following relation:

$$F-F_0=-\int_{V_0}^{V}P^*(V')dV'=\int_{\rho_0}^{\rho}P^*(\rho')/\rho'^2 d\rho' \ . \quad (5)$$

F_0 is an integration constant that needs to be known in order to determine the difference in free energy between state points separated by a first-order transition.

The integration over $P^*(\rho)$ can be carried out by fitting $P^*(\rho)$ to a convenient analytical form. For this we used the y expansion[11]

$$P^*(\rho)=\sum_n C_n^* y^n \ . \quad (6)$$

Here

$$y=\frac{\eta}{1-\eta} \quad (7)$$

and

$$\eta=v_0\rho \ , \quad (8)$$

where v_0 is the molecular volume.

For the liquid phase F_0 can be determined by comparing the free energy of a system with the free energy of an ideal gas. At low densities the difference in free energy between the two systems should disappear.

For the smectic and solid phase F_0 can be determined by thermodynamic integration to a system with known free energy. This will now be discussed.

Solid phase. For the solid phase the "reference system" is the fixed center-of-mass Einstein crystal. The free energy of this system is given by

$$F_E=-kT\ln\left[\int\sum_i \exp[-\beta\lambda_1(\mathbf{r}_i-\mathbf{r}_i^0)^2] \times\delta\left[\sum_i(\mathbf{r}_i-\mathbf{r}_i^0)\right]d(\mathbf{r})\right] -kT\ln\left[\int\sum_i\exp(-\beta\lambda_2\sin^2\theta_i)d(\Omega)\right] \ . \quad (9)$$

Here λ_1 and λ_2 are the coupling parameters which determine the strength of the harmonic force constants. The reason why the center of mass is kept fixed is discussed in Ref. 12.

The Helmholtz free energy of the Einstein crystal is known in closed form. For large values of λ_1 and λ_2 it is approximately given by

$$F_E\approx -kT\ln\left[N^{-3/2}\left(\frac{\pi}{\beta\lambda_1}\right)^{3/2(N-1)}\left(\frac{2\pi}{\beta\lambda_2}\right)^N\right] \quad (\lambda_{1,2}\to\infty) \ . \quad (10)$$

The free energy of the original system can be related to the free energy of the Einstein crystal by thermodynamic integration to the Einstein crystal, using a Hamiltonian

for a system of hard spherocylinders in a harmonic field,

$$H_{\lambda_1,\lambda_2}=H_0+\lambda_1\sum_i(\mathbf{r}_i-\mathbf{r}_i^0)^2+\lambda_2\sum_i\sin^2\theta_i\ , \tag{11}$$

When λ_1 and λ_2 become large, the contribution of H_0 to the free energy of this system becomes negligible. We therefore have

$$\begin{aligned}F_0&=F(\lambda_1=0,\lambda_2=0)\\&=F_E(\lambda_{1,m},\lambda_{2,m})-kT\ln V\\&\quad-\int_0^{\lambda_{1,m}}d\lambda_1\left\langle\sum_i(\mathbf{r}_i-\mathbf{r}_i^0)^2\right\rangle_{\lambda_1,\lambda_2}\\&\quad-\int_0^{\lambda_{2,m}}d\lambda_2\left\langle\sum_i\sin^2\theta_i\right\rangle_{\lambda_1,\lambda_2}(\lambda_{1,m},\lambda_{2,m}\to\infty)\ .\end{aligned} \tag{12}$$

Here the averages are taken with respect to the Hamiltonian H_{λ_1,λ_2}. Also in these averages, the center of mass is kept fixed. In order to get the free energy with respect to the "laboratory frame," a factor $-\ln V$ has to be added.[12] In practice, the integrals are performed by choosing a suitable path, i.e., we choose a parametrization

$$\lambda_1=\lambda_1(\xi),\quad \lambda_2=\lambda_2(\xi) \tag{13}$$

such that

$$\xi=-1\leftrightarrow\lambda_1=\lambda_2=0,\quad \xi=1\leftrightarrow\lambda_1=\lambda_{1,m},\quad \lambda_2=\lambda_{2,m}\ . \tag{14}$$

We then have

$$\begin{aligned}F_0&=F_E-\ln V\\&\quad-\int_{-1}^{1}d\xi\left[\left[\frac{d\lambda}{d\xi}\right]\left\langle\sum_i(\mathbf{r}_i-\mathbf{r}_i^0)^2\right\rangle_{\lambda_1,\lambda_2}\right.\\&\qquad\left.-\left[\frac{d\lambda_2}{d\xi}\right]\left\langle\sum_i\sin^2\theta_i\right\rangle_{\lambda_1,\lambda_2}\right]\\&\quad-\langle\exp(-\beta H_0)\rangle_{E,\lambda_{1,m}\lambda_{2,m}}\ .\end{aligned} \tag{15}$$

In the last term the average is taken over the Hamiltonian of the Einstein crystal. This term represents the difference in free energy between the system with Hamiltonian H_{λ_1,λ_2} at $\lambda=\lambda_{1,m}$, $\lambda_2=\lambda_{2,m}$ and the Einstein crystal at the same values of λ_1 and λ_2. For large values of $\lambda_{1,m}$ and $\lambda_{2,m}$ it can be shown to be equal to[12]

$$\langle\exp(-\beta H_0)\rangle_{E,\lambda_{1,m},\lambda_{2,m}}=\frac{N}{2}P_0\ . \tag{16}$$

Here, the average is taken over the Hamiltonian of the Einstein crystal, and P_0 is the probability for a particle to overlap with another particle, when the system evolves according to the Einstein Hamiltonian. If $\lambda_{1,2}\to\infty$, P_0 will vanish. For large values of $\lambda_{1,2}$, P_0 can be calculated by Monte Carlo simulation.

Smectic phase. For the smectic phase we chose as a reference system the system of parallel hard spherocylinders. The free energy of this system has been calculated in Ref. 3. A "free" smectic state is transformed into a parallel state by adding an aligning field to the Hamiltonian

$$H_\lambda=H_0(\mathbf{r}_i,\theta_i)+\lambda\sum_i\sin^2\theta_i\ . \tag{17}$$

It can now be shown that, for large λ_m,

$$\begin{aligned}F_0&=F_\lambda(\lambda=0)\\&=F_\lambda^{\rm id}(\lambda=0)+[F_\lambda(\lambda=\lambda_m)-F_\lambda^{\rm id}(\lambda=\lambda_m)]\\&\quad-N\int_0^{\lambda_m}(\langle\sin^2\theta\rangle_\lambda-\langle\sin^2\theta\rangle_{{\rm id},\lambda})d\lambda\\&\quad+kT[\ln\langle\exp(-\beta H_p)\rangle_\lambda-\ln\langle\exp(-\beta H_0)\rangle_{p,\lambda}]\ .\end{aligned} \tag{18}$$

Here $F_\lambda^{\rm id}$ is the rotational part of the free energy of an ideal gas of N rotators which has as a Hamiltonian

$$H_\lambda^{\rm id}(\theta_i)=\lambda\sum_i\sin^2\theta_i\ . \tag{19}$$

Hence

$$F_\lambda^{\rm id}=-NkT\ln\int_0^{2\pi}\int_0^{\pi}\exp(-\beta\lambda\sin^2\theta)(\sin\theta)d\theta\,d\phi\ . \tag{20}$$

The averages in the integral are the averages of a system of spherocylinders in the aligning field, and a system of rotators with the Hamiltonian $H_\lambda^{\rm id}$. In the averages in the logarithmic terms, the second average is taken over the Hamiltonian of a system of hard parallel spherocylinders with an "additional aligning field"

$$H_{p,\lambda}=H_p(\mathbf{r}_i)+\lambda\sum_i\sin^2\theta_i\ . \tag{21}$$

Note that H_p does not depend on θ_i. $H_{p,\lambda}$ can be regarded as the Hamiltonian of a system of parallel hard spherocylinders with an internal degree of freedom, which couples to an external aligning field.

Now we have

$$F_\lambda^{\rm id}(\lambda=0)=-NkT\ln 4\pi\ . \tag{22}$$

Furthermore,

$$\lim_{\lambda\to\infty}F_\lambda(\lambda=\lambda_m)-F_\lambda^{\rm id}(\lambda=\lambda_m)=F_p\ . \tag{23}$$

We see here that in order to obtain the free energy of the system of free cylinders we have to supply a strongly aligning field to the system, so that the particles become parallel. This takes an infinite amount of "aligning energy." The difference between this aligning energy and the aligning energy of a system of ideal rotators is, however, a finite quantity, which is just the free energy of the hard parallel spherocylinder system.

Now, for the third term

$$\begin{aligned}&kT[\ln\langle\exp(-\beta H_p)\rangle_\lambda-\ln\langle\exp(-\beta H_0)\rangle_{p,\lambda}]\\&\qquad=-N\int_{\lambda_m}^{\infty}[\langle\sin^2\theta\rangle_\lambda-\langle\sin^2\theta\rangle_{{\rm id},\lambda}]d\lambda\ .\end{aligned} \tag{24}$$

This will give a vanishingly small contribution if we choose λ_m large enough. If we now choose a suitable path

TABLE IV. Coefficients for the y expansion fits to the equation-of-state data. The range of validity is given in column 3. For the liquid phases, the exact C_1^*, C_2^*, and C_3^* are used, which are related to the virial coefficients by Eq. (32).

L/D	Phase	ρ^*	C_1^*	C_2^*	C_3^*	C_4^*	C_5^*
1.0	liquid	0.20–0.70	1.000	3.600	4.140	−1.654	0.5511
	solid	0.70–0.90	8.988	−3.467	1.542		
3.0	liquid	0.20–0.64	1.000	5.455	8.520	−7.670	2.471
	smectic	0.62–0.68	−4.086	15.429	−5.112		
	solid	0.66–0.90	6.770	−0.980	0.555		

$$\lambda=\lambda(\xi),\quad \lambda=0\leftrightarrow\xi=1,\quad \lambda=\infty\leftrightarrow\xi=-1\ , \tag{25}$$

we have

$$F_0=-NkT\ln 4\pi+F_p$$
$$+N\int_{-1}^{1}[\langle\sin^2\theta\rangle_\lambda-\langle\sin^2\theta\rangle_{\mathrm{id},\lambda}]\left|\frac{d\lambda}{d\xi}\right|d\xi\ . \tag{26}$$

The integral over $\langle\sin^2\theta\rangle_{\mathrm{id},\lambda}$ is known in closed form, and can be calculated directly. It turned out, however, that for $\lambda>1000$, when both terms in the integrand were determined separately, the difference between the two terms became smaller than the statistical error in the first term. We therefore used a method to determine the difference directly: we calculated both terms "simultaneously" in a MC program in the following way. For each particle we generated values of θ_i directly from the probability distribution

$$P(\theta)\propto\exp(-\beta\lambda\sin^2\theta)\ . \tag{27}$$

In this way, the term $\langle\sin^2\theta\rangle_{\mathrm{id},\lambda}$ can be determined numerically. We now used these θ_i also as the new trial values for a particle displacement in the MC algorithm of the system with Hamiltonian H_λ. The translational displacements in the MC step were still generated in the usual way. Now, if no overlap occurs after the trial step, the value of θ_i is a "good" value both for the system with Hamiltonain H_λ and for the system with Hamiltonian H_λ^{id}. In this case we have

$$\sin^2_{H_\lambda}\theta_i-\sin^2_{H_\lambda^{\mathrm{id}}}\theta_i=0\ . \tag{28}$$

If overlap occurs, the H_λ system retains its old value of λ, whereas in the H_λ^{id} system a new value occurs. In this case, the difference between the two terms is equal to

$$\sin^2_{H_\lambda}\theta_i-\sin^2_{H_\lambda^{\mathrm{id}}}\theta_i=\sin^2\theta_{i,\mathrm{old}}-\sin^2\theta_{i,\mathrm{new}}\ . \tag{29}$$

Now the statistical error in the difference is always smaller than the difference itself. Thus we are able to determine the integrand of Eq. (26) with greater accuracy.

Once we have obtained the absolute free energies for the various phases, the phase coexistence densities can be obtained. At these densities the following relations should hold:

$$P_I=P_{II},\quad G_I=G_{II}\ . \tag{30}$$

Here G is the Gibbs free energy, defined by

$$G=F+PV\ . \tag{31}$$

2. Results

$L/D=1$. The coefficients to the y expansion of the P^* for the liquid and the solid phase are given in Table IV. For the liquid phase, C_1^*, C_2^*, and C_3^* are the exact values, derived from the virial coefficients given in Refs. 1 by

$$C_n^*=\sum_{k=0}^{n-1}\binom{n-1}{k}(-1)^{n-k-1}4^kB_{k+1}^*\ ,$$
$$B_n^*=B_n/B_2^{n-1}\ . \tag{32}$$

The absolute free energy F_0 of the solid was calculated at a density $\rho^*=0.82$ by the application of (15). The respective terms which constitute F_0 are given in Table V. Having obtained F_0 and P^* in analytical form, we were able to find the densities for which (30) is satisfied. These are given in Table VI.

$L/D=3$. The coefficients for the y fit for the respective phases are given in Table IV. For the determination of the solid free energy we made use of Eq. (15). The results are given in Table V. For the smectic phase we made use of (26). The respective terms are given in Table V.

TABLE V. Various terms composing the free energy F_0 of the solid and smectic phases as given by Eqs. (15), (16), and (26). Note that here the free energies are given per particle. $f_{E,p}$ is the energy of the Einstein crystal or the parallel system, depending on whether the phase is solid or smectic. Likewise, $\mp\int_{-1}^{1}$ denotes the contribution of the respective integral terms in (15) or (26). In column 3, the density at which the free energy is calculated is given.

L/D	Phase	ρ^*	$f_{E,p}$	$\mp\int_{-1}^{1}$	$\frac{1}{2}P_0$	$-\ln 4\pi$	$-(\ln V)/N$	f_0
1.0	solid	0.82	14.686	−6.06(3)	0.006		−0.039	8.59(3)
3.0	solid	0.82	18.576	−8.50(5)	0.006		−0.029	10.05(5)
	smectic	0.64	2.086	5.80(16)		−2.531		5.35(16)

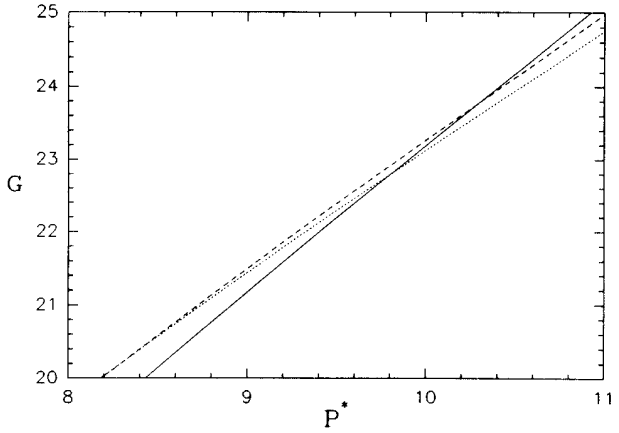

FIG. 6. Gibbs free energy G as a function of the pressure P^* for $L/D=3$. Here both G and P^* are determined by a y expansion with the coefficients given in Table IV. Solid line, isotropic liquid; dashed line, smectic; dotted line, solid.

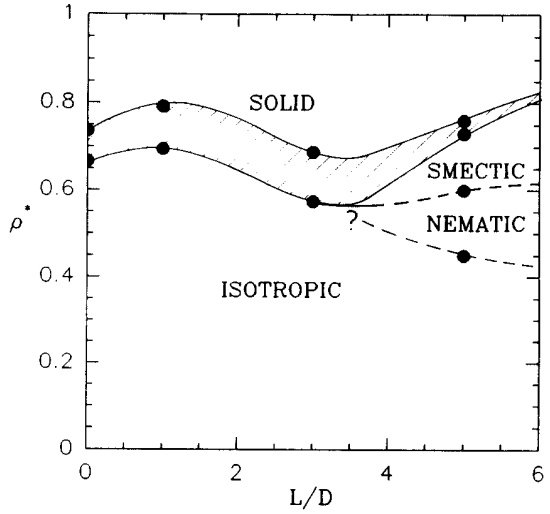

FIG. 7. Phase diagram for the hard-spherocylinder system. The dots denote the calculated coexistence points. The shaded region is the coexistence region. The isotropic-nematic-smectic triple point lies at a L/D ratio higher than 3.

From F_0 and P^* we once again found the coexistence densities. These are given in Table VI.

III. PHASE DIAGRAM AND DISCUSSION

From Table VI we see that, although we were able to create a mechanically stable smectic phase for $L/D=3$, this phase is not thermodynamically stable. Therefore, for $L/D=3$, as well as for $L/D=1$, the only stable phases are the isotropic and the solid phase. The coexistence pressure of the isotropic phase and the metastable smectic phase for $L/D=3$ are only slightly higher than the isotropic-solid coexistence pressure. We therefore expect that the smectic phase becomes thermodynamically stable at a L/D value which is only slightly higher than 3. As we do not observe a (metastable) nematic phase for $L/D=3$, we expect the nematic phase to become thermodynamically stable at a still higher L/D value. We therefore conjecture that the hard-spherocylinder phase diagram contains two triple points: an isotropic-smectic-solid triple point at L/D somewhat higher than 3, and an isotropic-nematic-smectic triple point at a higher value of L/D that is well below $L/D=5$. The latter prediction is somewhat higher than the predictions of density functional theory,[6,7] where an isotropic-nematic-solid coexistence point is predicted for $L/D \leq 3$.

It may appear strange that the isotropic-solid and isotropic-smectic transition densities are very close to each other (actually they are the same within error bars) whereas the isotropic-solid and smectic-solid transition densities show such a clear discrepancy. The reason for this becomes obvious when we look at a P^*-G plot for the three phases (Fig. 6); the solid and smectic lines are very nearly parallel, and close to each other in the considered region, resulting in intersection pressures (and hence densities) with the isotropic line that are very close to each other. The intersection pressures of the isotropic and smectic lines with the solid line are far apart, resulting in a large difference in the coexistence densities.

Combining our data with those of Refs. 5 and 8, we can now construct the tentative phase diagram for the hard-spherocylinder system. It is given in Fig. 7.

From Fig. 7 we see that for small values of L/D the coexistence region is located at a higher density than that of the hard-sphere system, contrary to the parallel hard-spherocylinder system, where the density decreases. The reason for this is that the free spherocylinder isotropic liquid has an extra rotational degree of freedom, which makes the entropy difference between the isotropic phase and the solid phase larger. The parallel system does not have such a rotational degree of freedom. In this system we have an entropy loss with respect to the hard-sphere

TABLE VI. Densities at which coexistence between the various phases occurs.

L/D	Transition	ρ_l^*	ρ_{sm}^*	ρ_{so}^*
1.0	liquid-solid	0.695(3)		0.792(2)
3.0	liquid-solid	0.574(3)		0.688(5)
	liquid-smectic	0.581(10)	0.665(10)	
	smectic-solid		0.624(66)	0.649(30)

system because of the greater excluded volume in the disordered (i.e., nematic) phase.

ACKNOWLEDGMENTS

We are indebted to R. Holyst and A. M. Somoza for sending us Refs. 7 and 6 prior to publication. This work is part of the research program of the Stichting voor Fundamenteel Onderzoek der Materie (Foundation for Fundamental Research on Matter) and was made possible by financial support from the Nederlandse Organisatie voor Wetenschappelijk Onderzoek (Netherlands Organization for the Advancement of Research).

[1]For a review of these simulations see T. Boublik and I. Nezbeda, Collect. Czech. Chem. Commun. **51**, 2301 (1986).

[2]D. Frenkel and B. M. Mulder, Mol. Phys. **55**, 1171 (1985).

[3]A. Stroobants, H. N. W. Lekkerkerker, and D. Frenkel, Phys. Rev. A **36**, 2929 (1987).

[4]W. L. McMillan, Phys. Rev. A **4**, 1238 (1971); A. Kloczkowski and J. Stecki, Mol. Phys. **55**, 689 (1985); F. Dowell, Phys. Rev. A **28**, 3526 (1983); Y. Maeda and S. Hachisu, Colloids Surf. **6**, 1 (1983); M. Hosino, H. Nakano, and H. Kimura, J. Phys. Soc. Jpn. **46**, 1709 (1979).

[5]D. Frenkel, H. N. W. Lekkerkerker, and A. Stroobants, Nature **332**, 822 (1988).

[6]A. Poniewierski and R. Holyst, Phys. Rev. Lett. **61**, 2461 (1988); Mol. Phys. (to be published).

[7]A. M. Somoza and P. Tarazona (unpublished).

[8]W. G. Hoover and F. H. Ree, J. Chem. Phys. **49**, 3609 (1968).

[9]See, e.g., M. P. Allen and D. J. Tildesley, *Computer Simulation of Liquids* (Oxford University Press, New York, 1987).

[10]J. Vieillard-Baron, Mol. Phys. **28**, 809 (1974).

[11]B. Barboy and W. M. Gelbart, J. Chem. Phys. **71**, 3053 (1979).

[12]D. Frenkel and A. J. C. Ladd, J. Chem. Phys. **81**, 3188 (1984).